Article

An Object-Based Approach for Fire History Reconstruction by Using Three Generations of Landsat Sensors

Thomas Katagis [1],*, Ioannis Z. Gitas [1] and George H. Mitri [2]

[1] Laboratory of Forest Management and Remote Sensing, Aristotle University of Thessaloniki, P.O. Box 248, GR 54124 Thessaloniki, Greece; E-Mail: igitas@for.auth.gr

[2] Institute of the Environment, University of Balamand, P.O. Box 100, Tripoli, Lebanon; E-Mail: george.mitri@balamand.edu.lb

* Author to whom correspondence should be addressed; E-Mail: thkatag@for.auth.gr; Tel.: +30-2310-992-701; Fax: +30-2310-992-699.

Abstract: In this study, the capability of geographic object-based image analysis (GEOBIA) in the reconstruction of the recent fire history of a typical Mediterranean area was investigated. More specifically, a semi-automated GEOBIA procedure was developed and tested on archived and newly acquired Landsat Multispectral Scanner (MSS), Thematic Mapper (TM), and Operational Land Imager (OLI) images in order to accurately map burned areas in the Mediterranean island of Thasos. The developed GEOBIA ruleset was built with the use of the TM image and then applied to the other two images. This process of transferring the ruleset did not require substantial adjustments or any replacement of the initially selected features used for the classification, thus, displaying reduced complexity in processing the images. As a result, burned area maps of very high accuracy (over 94% overall) were produced. In addition to the standard error matrix, the employment of additional measures of agreement between the produced maps and the reference data revealed that "spatial misplacement" was the main source of classification error. It can be concluded that the proposed approach can be potentially used for reconstructing the recent (40-year) fire history in the Mediterranean, based on extended time series of Landsat or similar data.

1. Introduction

Forest fires are considered to be one of the major factors affecting vegetation succession, and nutrient and global carbon cycles [1,2]. In addition, they potentially contribute to biodiversity loss, soil erosion, and degradation processes [3,4]. Understanding the behavior and interaction of forest fires with different ecosystems is important for analyzing spatial and temporal patterns of fire occurrence, as well as for studying changes in ecosystem functions [5,6]. While, historically, fire regimes have been mainly influenced by human activities and practices [7], more recently, climatic and environmental changes are also considered as driving factors affecting fire occurrence and vegetation succession [8,9]. These constantly evolving interactions and effects of fire in space and time constitute what is referred in the literature as fire history [10].

Collection of reliable fire statistics and generation of time series of burned area maps become essential when the fire history of a certain area is considered [5,11]. Accurate reconstruction of fire history is related, among others, to the following:

- investigation and monitoring of the long-term post-fire vegetation succession [12],
- understanding of the causes of fire ignition [13],
- investigation of the interactions between climate change and fire occurrence [11],
- preservation and management of biodiversity [14], and
- determination of pre-fire planning and other fire management related policies [15].

However, the consistency of fire statistics varies according to the spatial and temporal scale of interest, the collection method, and the organization they are delivered by [11,16]. Given the increase in the number of extreme fire events over the past decades, in many parts of the world, and especially in the Mediterranean region [12], delivering accurate and timely-consistent fire statistics has become important for national, as well as international, organizations (e.g., national forest services, EUROSTAT, European Forest Fire Information System, Food and Agriculture Organization).

Satellite remote sensing has been widely employed for fire history reconstruction both at the local/regional/national [17,18], as well as the continental/global [19,20], level. More specifically, the most recent (post-2000) global fire history reconstruction is based mainly on the use of MODIS [20,21] and SPOT VEGETATION [22] data, while the creation of fire history over longer time periods involved the extensive use of the Advanced Very High Resolution Radiometer (AVHRR) [11,23]. Despite the limitations of these sensors due to detection capabilities and sampling inconsistencies [16], they constitute the primary source for producing global records of fire activity. At a local/regional scale where more detailed information is required, satellite data with higher spatial resolution could constitute an alternative, and, often, the only available source of information, for the reconstruction of the recent and sometimes longer fire history of an area.

With a more than 40-year archive covering the globe with moderate resolution (30–80 m) multispectral data provided at low or zero cost, the Landsat sensors have significantly contributed to land management [24]. Indeed, since the initiation of the Landsat satellite program, numerous land management projects, including fire-related ones, have been based on data from the three main sensors on board the different Landsat satellites, namely the Multispectral Scanner (MSS), the Thematic (TM), and Enhanced Thematic Mapper (ETM+) sensors [15,18,25]. The recent launch of Landsat-8, as part

of the Landsat Data Continuity Mission (LDCM) [26], ensures open access to Landsat data for the coming years, both for operational and scientific applications. Consequently, these time series of archived and newly acquired Landsat images offer the potential of reconstructing fire history not only at local/regional but also at a global scale with improved spatial accuracy.

A prerequisite of recreating the fire history of an area is the detection of fire scars and the accurate mapping of the burned areas. Along with the abundance of satellite data, numerous approaches and techniques have been developed for detection and mapping of burned areas including: vegetation index differencing [27,28], Principal Component Analysis (PCA) [29], Spectral Mixture Analysis (SMA) [30], logistic regression [31], supervised classification [17], and multitemporal image compositing [32]. In addition, advanced image analysis techniques, such as neural networks [33] and support vector machines [34], have also been employed. According to Katagis *et al.* [35], the selection of an appropriate procedure or technique depends on the aim of the study, data availability and ecosystem characteristics. Existing automated or semi-automated procedures for detection and mapping of burned areas are based mainly on low-resolution data with high temporal frequency, such as AVHRR and MODIS [19,20,36]. In contrast, semi-automated procedures that employ medium to high spatial resolution data are considerably fewer and are mainly developed with the use of Landsat imagery [12,37–39].

The majority of the conducted research, created products, and developed services rely, thus far, on pixel-based (spectral) information and the related image analysis techniques. However, recently, the use of objects (instead of pixels) that can facilitate the usage of, not only spectral, but also contextual and spatial information, considering the shape and texture of objects, as well as topological features (neighbor, super-objects, *etc.*), has been developed [40,41]. Geographic object-based image analysis (GEOBIA) has been devoted to developing automated methods of partitioning high-resolution, remote-sensing imagery into meaningful image-objects, and assessing their characteristics through a scale [42]. A semi-automated GEOBIA procedure with Landsat TM data was proposed by Mitri and Gitas [37] for mapping burned areas in the Mediterranean region. GEOBIA of optical satellite data, ranging from low to very high spatial resolution, has been successfully used for burned area mapping, resulting in high classification accuracies [43–45]. The findings of these studies also demonstrated that confusion between burned areas and other land cover classes were significantly minimized.

Based on the above, it would be worth exploring the capability of GEOBIA for the generation of time series of burned area maps with the use of past and current Landsat acquisitions. The aim of this work was to develop an object-based model that would take advantage of the Landsat image availability in order to reconstruct recent (30 years) fire history in a typical Mediterranean environment. For this purpose, data from the Multispectral Scanner (MSS), the Thematic Mapper (TM), and the Operational Land Imager (OLI) sensors were employed. The specific objectives were:

- to develop an object-based classification model for mapping in detail burned areas using the TM scene for which accurate official fire perimeter provided by the Greek Forest Service was available;
- to test the transferability of the developed model by applying it to the MSS and OLI images in order to investigate the potential of the proposed method to be used operationally for the reconstructions of the recent fire history of the study area.

2. Study Area and Dataset Description

The study area of the Mediterranean island of Thasos in Greece was used to develop and test the model for creating these times series of burned area maps. Thasos is Greece's most northerly island, extending from 24°30′ to 24°48′E and 40°33′ to 40°49′N, with a surface area of 399 km² and a perimeter of approximately 102 km (Figure 1). Elevation ranges from sea level to 1217 m. *Pinus brutia* is the dominant tree species at lower elevations (0 to 800 m), whereas *Pinus nigra* is found at higher altitudes [46]. In addition, other types of Mediterranean vegetation, such as maquis and garrigue (a scrubland vegetation of the Mediterranean region composed primarily of leathery broad-leaved evergreen shrubs or small trees), are also present. The dry/hot season (xerothermic period) starts in May and lasts for four to five months, up to mid-September, with August being the driest and July the warmest month of the year.

Figure 1. Location of Thasos Island and the Landsat images used in the study.
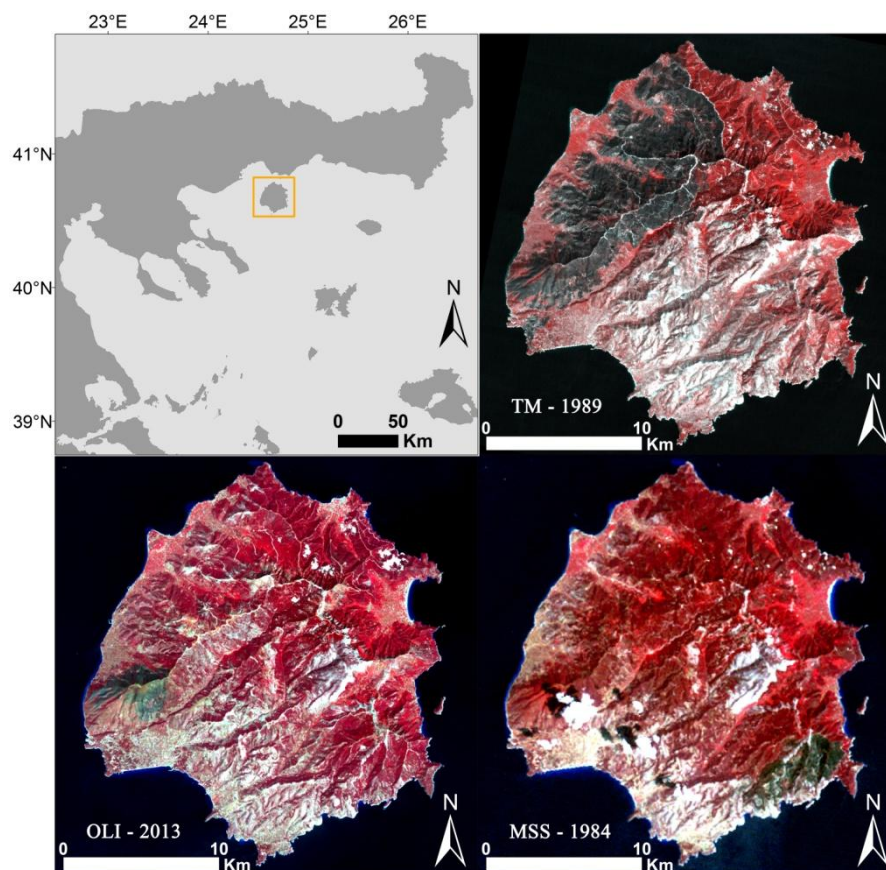
The island of Thasos has been severely damaged by forest fires during the last 30 years, almost in its entirety. Before the large forest fire of 1984, forest and forested lands covered 47.5% of the island [47], making forests the dominant land cover type at the time. After the fires of 1984 and 1985, forests and forested lands were reduced to 37.95% of the island [47]. The present study focuses on the fires during the summers of 1984, 1989, and 2013.

Three Landsat images were used, that were acquired soon after the fire events in the study area. More specifically, MSS, TM, and OLI images acquired on 4 August 1984, 19 September 1989, and 20 August 2013, respectively, were collected (Table 1). Ancillary data utilized for pre-processing

of the data and validation of the classification results were: the official forest service perimeters of the fires in Thasos, field data when available, a 1:50,000 topographic map and a 10 m digital elevation model (DEM) of Thasos. In addition, three pre-fire Landsat images were used respectively to further assist the validation procedure only, as it is described in the following sections.

Table 1. Description of Landsat imagery used in this study.

Landsat Data	Spatial Resolution	Acquisition Date	Date of Fire Event	Area (ha)
Landsat 5 MSS	60 m	1984-08-04	1984-07-21	1605
Landsat 5 MSS (pre)	60 m	1984-06-26		
Landsat-4 TM	30 m	1989-09-19	1989-08-16	9560
Landsat-4 TM (pre)	30 m	1989-07-09		
Landsat-8 OLI	30 m	2013-08-20	2013-08-16	818
Landsat-8 OLI (pre)	30 m	2013-08-04		

3. Methodology

In the following subsections the methodology steps are presented in detail. The methodology comprised pre-processing of the satellite data, development of the object-based classification model with the use of the TM image, application of the model to the other two images, and, finally, the accuracy assessment of the produced burned area maps.

3.1. Data Pre-Processing

Initially, the Landsat images were ortho-rectified with the use of the DEM and the 1:50,000 topographic map of the island as reference map. The correction involved identification of ground central points (GCPs) in the Landsat images and on the topographic map. The images were then reprojected into the EGSA projection system (Greek grid) using a bilinear interpolation. The statistical technique of least squares regression was used to determine the coefficients for the coordinate transformation equations. The total RMS errors associated with the GCPs were lower than 0.6 pixels for all images.

The MSS and TM image values were converted from raw Digital Numbers (DN) to Top of the Atmosphere (ToA) reflectance by using the calibration coefficients and equations, as described by Chander *et al.* [48]. The OLI image was likewise converted to ToA reflectance following the procedure described in the USGS Landsat mission website (https://landsat.usgs.gov/Landsat8_Using_Product.php). Moreover, the images were corrected for atmospheric effects by applying the Dark Object Subtraction (DOS) technique, which is one of the most-widely used, and simplest, absolute atmospheric correction approaches [49,50]. Although atmospheric correction is not always required when single date images are analyzed, applying a basic correction was considered useful for improving the classification performance.

3.2. Development of the GEOBIA Classification Model

The object-based classification model was developed with the use of the 1989 Landsat TM image [37] by employing the software eCognition Developer 8. The 1989 image was initially selected for building the model due to the availability of accurate fire reference data for that year. The

transferability of the model was tested and assessed using the 1984 MSS image and the 2013 OLI image consecutively. The object-based image analysis involved two steps, namely segmentation and classification, where the generated image objects were classified according to class descriptions organized in an appropriate knowledge base. In the development process few modifications and changes from the initially developed model with the TM scene [42] were performed, in order to accommodate changes in the characteristics of the other satellite images. The basic processes of the initial model development and the subsequent modifications are described below (Figure 2).

Figure 2. Flowchart of the methodology steps followed for the development of the GEOBIA classification model. This was initially developed with the use of the TM image. Minor modifications were performed when applied to the other Landsat images.
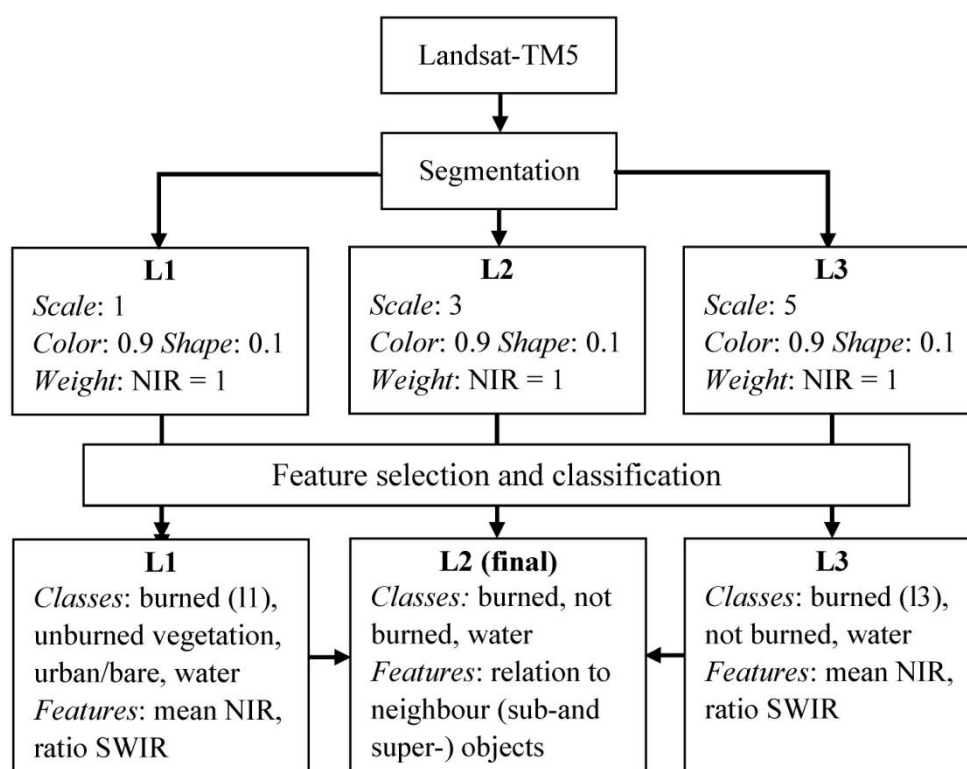

The strategy before classifying the burned area was to create a three-level graded scale of segmentation in a bottom up region-merging approach, starting with one-pixel objects. The near-infrared (NIR) spectral band was used for segmenting the images. The multi-resolution segmentation results were used to construct a hierarchical network of image objects that simultaneously represented image information at different spatial resolutions. Thus, the smaller objects at level 1 (regarded as sub-objects) and the larger objects at level 3 (regarded as super-objects) provided information for the final classification of objects at level 2.

In order to generate the optimum, in terms of homogeneity, segments for the classification, several parameters had to be adjusted. These included the scale of the objects, the weights of the single layers and the heterogeneity criterion. Scale remains one of the most important factors for image understanding, since an image object may appear differently or not at all depending on various levels of scales [45]. Consequently, in this work, the optimum scale for the object analysis was determined according to the

classification purpose, with the largest objects created at scale 5. The weight defined the degree of information from each selected layer to be considered for the segmentation process. Regarding the heterogeneity criterion, this included the gray tone (color), as expressed by the digital value of the objects, and shape (textural homogeneity) primary object features, with the latter consisting of two sub-criteria, smoothness and compactness of objects. Considering this multi-resolution segmentation as an optimization process, the main goal was to minimize the spectral heterogeneity of the generated objects.

Figure 3. Classification of objects at level 2 as burned (in yellow), not burned (in green) and water (in blue) for the MSS (**a**) and OLI (**b**) images of Thasos. Membership functions of ratios of NIR (**c**) and SWIR (**d**) for classifying "burned" at level 2 are displayed for the OLI image.

(a)   (b)

(c)   (d)
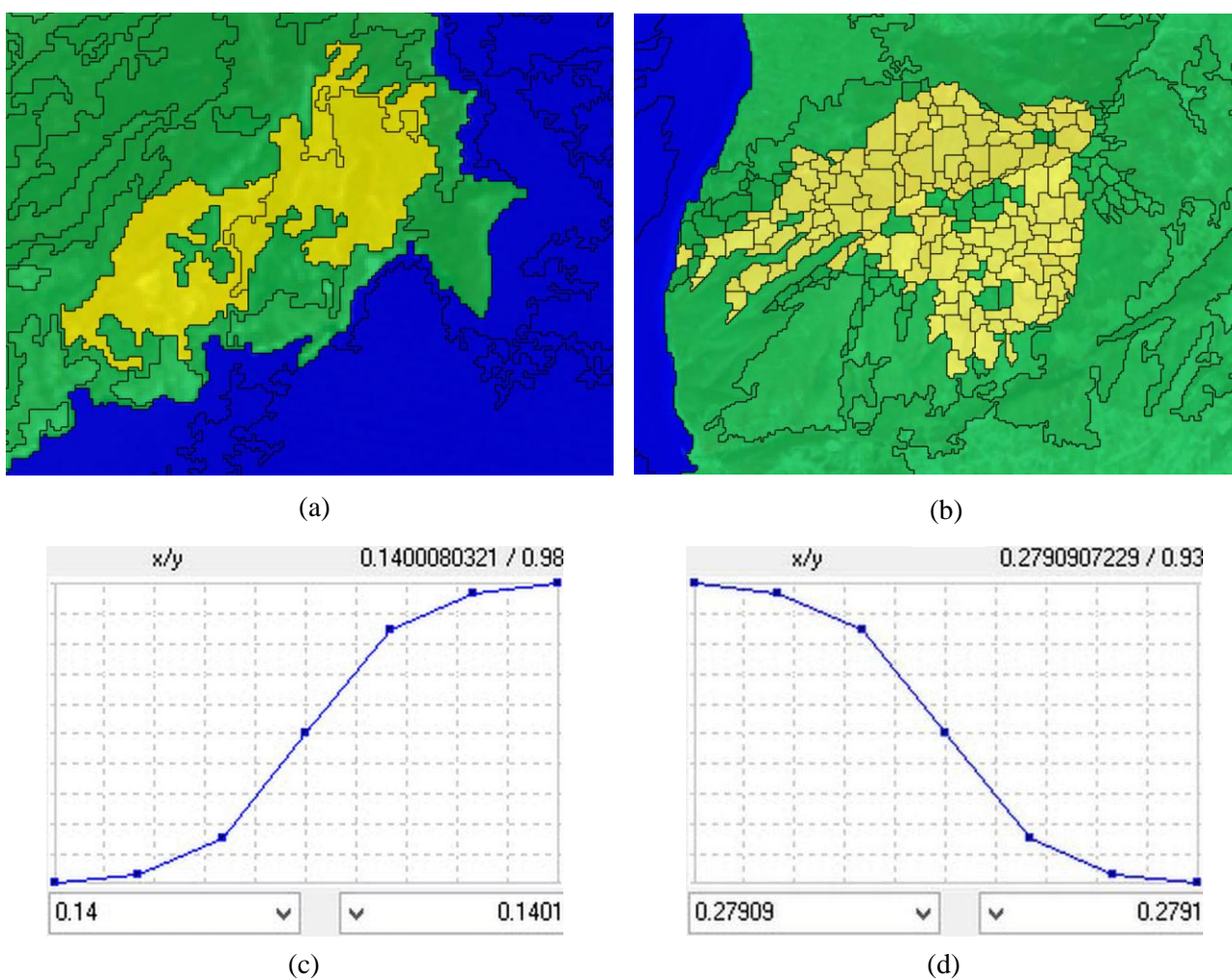
The next step was to perform classification of the resulting objects. The classification was based on fuzzy logic, where each class contains a class description and a class description can consist of a set of fuzzy expressions. The fuzzy sets are defined by membership functions that identify those values of a feature that are regarded as typical, less typical, or not typical of a class, *i.e.*, they have a high, low, or zero membership, respectively, of the fuzzy set. Therefore, for each class a rule was defined, which comprised one or a combination of features (conditions) that had to be fulfilled for an object to be assigned to a class.

Classification at level 1 included the following classes: "burned (l1)", "unburned vegetation", "urban/bare", and "water", while classification at level 3 included the following classes: "not burned", "burned (l3)", and "water". The final classification of the burned area at level 2 was based on the information of objects classified as burned at levels 1 and 3. Through this hierarchical network at the different scales each image object "knows" its sub- and super-objects allowing for a more precise analysis of the class objects. The main features selected for the classification were the mean values and ratios of the NIR (0.76–0.90 μm) and SWIR (2.08–2.35 μm) bands of the TM image. Layer mean value $\bar{c}_L$ is calculated from the layer values c_{Li} of all n pixels forming an image object, whereas the ratio r_L is the layer L mean value of an image object $\bar{c}_{LO}$ divided by the sum of all layer mean values of the object $\bar{c}_{LSO}$ [51]:

$$\bar{c}_L = \frac{1}{n} \sum_{i=1}^{n} c_{Li} \tag{1}$$

$$r_L = \frac{\bar{c}_{LO}}{\bar{c}_{LSO}} \tag{2}$$

The developed model was finally applied to the MSS and OLI images, where the segmentation parameters, regardless of the different spatial resolution of the MSS, and class structure were retained (Figure 3). Modifications in the ruleset were performed for mapping the 1984 fire, since the MSS image lacked the SWIR band and analysis relied on information from mean value of the red, blue and ratio of the NIR spectral bands. Regarding the OLI image, the model was applied likewise after adjusting the feature values, namely mean and ratio values of NIR (0.85–0.88 μm) and SWIR (2.11–2.29 μm), in the membership functions.

3.3. Validation of the Burned Area Maps

The validation of the burned area maps was based on the estimation of the error matrix for each classification. The error matrix, one of the most common methods to assess the accuracy of thematic maps, generates descriptive statistics for the overall accuracy of the product as well as for the omission and commission errors (Oe, Ce) of the desired class [52]. Based on the error matrix, two summary measures were also computed, the quantity and allocation disagreement [53,54]. After analyzing various Kappa indices of agreement and comparing the standard Kappa with the disagreement components in selected published literature, Pontius and Millones [54] concluded that the latter measures are simpler and much more convenient for summarizing the estimated error matrix in remote sensing applications. Quantity disagreement between the reference and the produced map occurs when the number of pixels for each category is different in the two maps, while allocation disagreement is caused by mismatch in the spatial allocation of the pixels of each category. These measures are expressed by the following equations, where *Q* and *A* are the overall quantity and allocation disagreement of all categories *J*, respectively, q_g is the quantity disagreement for an arbitrary category *g*, a_g is the allocation disagreement of category *g*, and *p* expresses the proportion of each category in the error matrix [54] (Pontius and Millones 2011):

$$Q = \frac{\sum_{g=1}^{J} q_g}{2} \tag{3}$$

$$q_g = \left| \left(\sum_{i=1}^{J} p_{ig} \right) - \left(\sum_{j=1}^{J} p_{gj} \right) \right| \tag{4}$$

$$A = \frac{\sum_{g=1}^{J} a_g}{2} \tag{5}$$

$$a_g = 2\min\left[\left(\sum_{i=1}^{J} p_{ig} \right) - p_{gg,} \left(\sum_{j=1}^{J} p_{gj} \right) - p_{gg} \right] \tag{6}$$

The validation procedure was based on random sampling meaning that every pixel, which is considered here as the sampling unit, had the same chance of being included in the sample, regardless of the final classification map. A total of 150 pixels were selected from each classified image and compared with the reference data for validating each map. The sample size was considered statistically sound, as suggested by Czaplewski [55], considering a desired accuracy of at least 90% with a maximum allowed error of 5%. Ideally, the results of the OBIA classification should be validated with the use of objects as sampling units, in order to reduce inherent point-based approach errors, such as geolocation inaccuracy [56], although there is no standard method generally adopted in the literature. However, selection of consistent reference objects would be still a challenging task if we consider that: (i) the field surveys conducted after the three fires were not based on an object-oriented response design; and (ii) photo-interpretation of the images could still not ensure the generation of homogeneous reference segments, especially for the 60-m resolution MSS image.

It should be mentioned that the official fire perimeters did not include unburned patches inside the polygons. It is quite common that the reference maps provided by the forest services are based on rough delineations leading to over- or under-reporting of areas burned, which affects the validation results [57]. Hence, in order to assist the creation of more accurate reference data, the Normalized Burn Ratio (NBR) (Equation (7)) and Normalized Difference Vegetation Index (NDVI) (Equation (8)) indices were calculated for the pre- and post- fire Landsat images and spectral image differencing was applied. The resulting differenced Normalized Burn Ratio (dNBR) (Equation (9)) [58] and the differenced Normalized Difference Vegetation Index (dNDVI) (Equation (10)) [59] allow for a more clear discrimination between burned and unburned vegetation. The NDVI was used for the MSS images, since short-wave infrared (SWIR) (2.08–2.35 μm) spectral bands are only available in the TM, OLI sensors. NIR (0.76–0.90 μm) and RED (0.63–0.69 μm) refer to the near infrared and red spectral bands, respectively. The index differencing was specifically applied for the validation step and was not considered for the model development.

$$NBR = \frac{NIR - SWIR}{NIR + SWIR} \tag{7}$$

$$NDVI = \frac{NIR - RED}{NIR + RED} \tag{8}$$

$$dNBR = NBR_{pre} - NBR_{post} \tag{9}$$

$$dNDVI = NDVI_{pre} - NDVI_{post} \tag{10}$$

4. Results and Discussion

The effectiveness of the developed GEOBIA model to map the burned areas, and thus reconstruct the recent fire history of the island, was assessed by comparing the classification results (Figure 4) with the reference data.

Figure 4. Burned area maps (in white) of the study area derived after applying the OBIA classification model. The forest service perimeters are displayed in black.
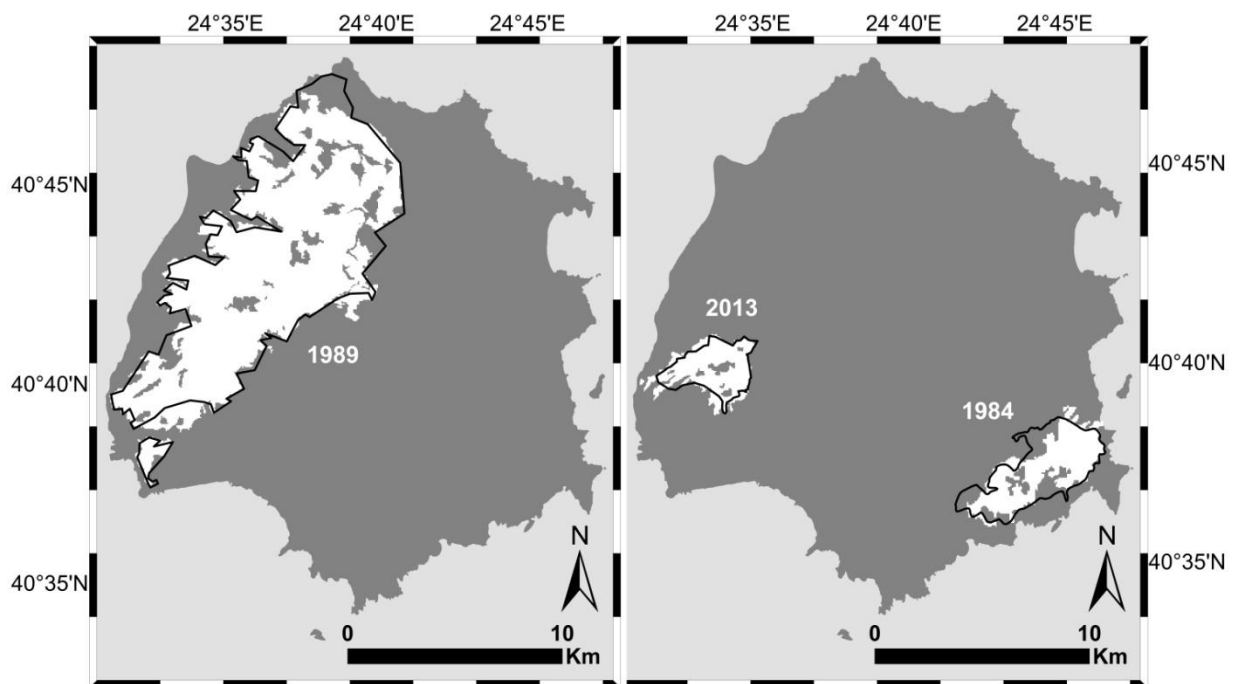
Initially, accuracy assessment was performed for the 1989 burned area. The descriptive statistics derived from the error matrix are presented in Table 2. The developed object-based image analysis procedure successfully mapped the burned area achieving an overall accuracy (OA) of 95.33%. The omission (Oe) and commission (Ce) errors were quite low (4.81% and 3.66%, respectively), with only three pixels being misclassified as unburned out of the 82 predicted as burned. Regarding the effectiveness of the model when applied to the TM and OLI images, high overall accuracies were also achieved for the fires of 1984 and 2013. In the fire of 1984 the number of misclassified pixels was higher overall when compared with the other two events, resulting in higher omission error (8.00%). This can be attributed to the lower spatial resolution of the MSS image used for classifying the burned area. High omission error (6.01%) was also observed in the burned area of 2013, where it seems that part of the predicted as unburned area was actually affected by the fire. In all classifications, omissions of the burned area are mainly caused by slightly burned, sparsely vegetated patches that were not mapped by the model. Still, the observed errors were low in all study areas and confusion between burned, shaded, and urban areas was successfully minimized.

Table 2. Accuracy assessment results for the classifications of the burned areas. Overall accuracy (OA), Omission (Oe), and Commission (Ce) errors are estimated based on the error matrix. The estimated size of the burned areas that were classified by the object-based image analysis is also presented.

| Classified | Reference | | OA (%) | Oe (%) | Ce (%) | Area (ha) |
	Burned	Unburned				
1984						
Burned	57	4	94.00	8.00	6.56	1214
Unburned	5	84				
Total	62	88				
1989						
Burned	79	3	95.33	4.81	3.66	8558
Unburned	4	64				
Total	83	67				
2013						
Burned	62	1	96.67	6.01	1.59	887
Unburned	4	83				
Total	66	84				

In addition to the standard statistics of the error matrix, the quantity and allocation disagreement components were derived for each case. These are an additional measure of agreement between two maps and quantify the differences in terms of the number and spatial mismatch of the pixels of a given category [58]. These components are displayed in Figure 5 and are expressed as the disagreement proportions for both burned and unburned classes. The overall accuracy or agreement proportion can be derived if the total disagreement proportion is subtracted from 1. The highest disagreement is estimated for the 1984 map (6%) while a 5% and 3% disagreement are estimated for the 1989 and 2013 maps, respectively. The quantity difference is equal to only 1% for the 1984 and 1989 maps, which accounts for less than 20% of the overall disagreement. For the 2013 map, we observe that quantity difference is slightly higher (2%) accounting for more than 50% of the total error, however these figures are still quite low. These results exhibit that the number of pixels predicted for each class do not differ substantially from the number of reference pixels. Even if the quantity disagreement was zero, meaning that the number of predicted and observed changes was equal, disagreement would still occur due to the assignment of pixels in the wrong class by the classifier. Consequently, these measures seem to provide a straightforward and more comprehensive way to summarize the error matrix and explain the source of error.

The combined use of spectral and contextual information in this GEOBIA approach significantly reduced errors related to the confusion of burned areas with other land cover classes. Additionally, the annoying "salt-and-pepper" effect appearing in pixel-based classifications was avoided. The advantages of applying fuzzy classification to image objects for mapping burned areas with Landsat imagery has been discussed in detail in the work of Mitri and Gitas [37]. In their work, a comparison between object and pixel-based classification results revealed also that the misclassified area in the object approach was considerably smaller.

Figure 5. Quantity and allocation disagreement components estimated for each classification. The components are expressed as proportions of burned and unburned classes.
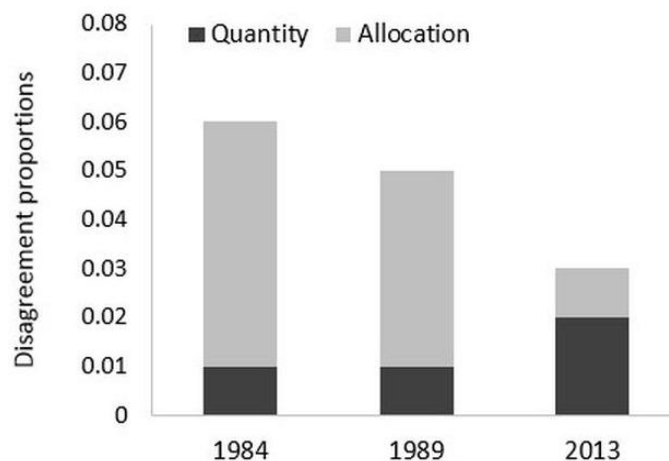
However, in order to accomplish this high classification performance, extraction of homogeneous segments was required. This is not always an easy task as the spatial resolution of the data and the topography of the study area can limit the extraction of highly homogeneous segments. Object delineation and segmentation procedures are facilitated in a 1-m resolution image, but this is not the case at 30 m or more. We should not neglect the fact that the specific benefits of GEOBIA were primarily emphasized in applications with very high-resolution data, before object-based procedures were applied to Landsat or other medium and coarse resolution data [41]. In this work the relatively homogeneous distribution of the burned areas assisted the segmentation and accordingly the classification performance, which has been also reported in a similar study [45].

It is worth mentioning that the features selected for classifying the burned areas involved only the mean and ratio values of the spectral bands of the single images. No additional image transformation, such as vegetation indices or image differencing, were needed to achieve these high accuracies overall. This does not mean, of course, that additional information would not further assist the analysis. Nonetheless, this indicates that the developed model can provide reliable results by integrating spatial and basic spectral information through a semi-automated procedure. Moreover, the process of applying the model to the other Landsat images did not require substantial tuning, thus, extended series of images could be processed with minor complexity for creating time series of burned areas maps.

The current acquisition plan of Landsat-8 ensures now that almost two images per month (16-day revisit) are available over a certain location, thus, assisting the selection of high-quality images to be used for rapid post-fire assessment on an operational basis. Obviously, in Mediterranean sites selection of the most suitable images is also favored by the availability of more cloud-free images, as opposed to higher latitude areas for example. Despite spatial and temporal discontinuities existing in the Landsat archive due to technology limitations and sensor failures, the Landsat time series consist, nowadays, the largest pool of medium resolution data for reconstructing the fire history of an area.

5. Conclusions

The main conclusion drawn from this work is that the developed object-based approach is capable of producing burned area maps of very high accuracy independently of the type of Landsat image

employed, and, therefore, has the potential to be used for the recent (40-year) fire history reconstruction of an area at the local/regional/national level.

More specifically, the developed OBIA model produced burned area maps of very high accuracy (over 94%) when it was tested on MSS, TM, and OLI images of the Mediterranean island of Thasos. It should be noted that supplementary measures of agreement between the produced maps and the reference data revealed "spatial misplacement" as the main source of the classification error estimated by the error matrix. This allocation disagreement occurs since the classifier predicts burned or unburned areas in wrong locations in the maps, and these predictions are then expressed as omission and commission errors. In addition, the proposed OBIA approach was proven efficient in minimizing the confusion between the burned areas and other land cover classes.

The proposed semi-automated approach which makes use of original spectral information and simple ratios found in the bands of all three sensors used in this study, proved to be easily transferable between MSS, TM, and OLI, without requiring any substantial adjustments to the spatial and spectral characteristics of the images. This is one of the advantages of the proposed approach when compared to multi-step approaches found in similar studies. The use of a complete time-series of Landsat images of an area with similar characteristics will be the next logical step in order to examine the applicability of the proposed approach as an operational tool for fire history reconstruction in the Mediterranean.

Acknowledgments

Author Contributions

All authors have made significant contributions to the manuscript. Thomas Katagis is the main author who wrote the manuscript, conducted pre-processing of the images, as well as the accuracy assessment of the maps. Ioannis Z. Gitas had the original idea, supervised the study, and contributed in manuscript writing and revision. George H. Mitri developed and applied the GEOBIA classification model and contributed in the manuscript revision.

Conflicts of Interest

The authors declare no conflict of interest.

References

1. Kutiel, P.; Inbar, M. Fire impacts on soil nutrients and soil erosion in a mediterranean pine forest plantation. *Catena* **1993**, *20*, 129–139.
2. Capitanio, R.; Carcaillet, C. Post-fire mediterranean vegetation dynamics and diversity: A discussion of succession models. *Forest Ecol. Manag.* **2008**, *255*, 431–439.

3. Pérez-Cabello, F.; de la Riva Fernández, J.; Montorio Lloverá, R.; García-Martín, A. Mapping erosion-sensitive areas after wildfires using fieldwork, remote sensing, and geographic information systems techniques on a regional scale. *J. Geophys. Res.: Biogeosci.* **2006**, doi:10.1029/2005JG000148.

4. Pausas, J.G.; Llovet, J.; Rodrigo, A.; Vallejo, R. Are wildfires a disaster in the mediterranean basin?—A review. *Int. J. Wildland Fire* **2008**, *17*, 713–723.

5. Díaz-Delgado, R.; Lloret, F.; Pons, X. Statistical analysis of fire frequency models for catalonia (NE Spain, 1975–1998) based on fire scar maps from Landsat MSS data. *Int. J. Wildland Fire* **2004**, *13*, 89–99.

6. Turner, M.G. Disturbance and landscape dynamics in a changing world. *Ecology* **2010**, *91*, 2833–2849.

7. Caldararo, N. Human ecological intervention and the role of forest fires in human ecology. *Sci. Total Environ.* **2002**, *292*, 141–165.

8. Pausas, J.; Fernández-Muñoz, S. Fire regime changes in the western mediterranean basin: From fuel-limited to drought-driven fire regime. *Clim. Chang.* **2012**, *110*, 215–226.

9. Moreno, M.V.; Conedera, M.; Chuvieco, E.; Pezzatti, G.B. Fire regime changes and major driving forces in spain from 1968 to 2010. *Environ. Sci. Policy* **2014**, *37*, 11–22.

10. Pyne, S.J. *Introduction to Wildland Fire: Fire Management in the United States*; John Wiley & Sons Inc.: New York, NY, USA, 1984.

11. Chuvieco, E.; Englefield, P.; Trishchenko, A.P.; Luo, Y. Generation of long time series of burn area maps of the boreal forest from NOAA–AVHRR composite data. *Remote Sens. Environ.* **2008**, *112*, 2381–2396.

12. Röder, A.; Hill, J.; Duguy, B.; Alloza, J.A.; Vallejo, R. Using long time series of Landsat data to monitor fire events and post-fire dynamics and identify driving factors. A case study in the Ayora region (eastern Spain). *Remote Sens. Environ.* **2008**, *112*, 259–273.

13. Loepfe, L.; Lloret, F.; Román-Cuesta, R.M. Comparison of burnt area estimates derived from satellite products and national statistics in Europe. *Int. J. Remote Sens.* **2011**, *33*, 3653–3671.

14. Bengtsson, J.; Nilsson, S.G.; Franc, A.; Menozzi, P. Biodiversity, disturbances, ecosystem function and management of European forests. *Forest Ecol. Manag.* **2000**, *132*, 39–50.

15. Lentile, L.B.; Holden, Z.A.; Smith, A.M.S.; Falkowski, M.J.; Hudak, A.T.; Morgan, P.; Lewis, S.A.; Gessler, P.E.; Benson, N.C. Remote sensing techniques to assess active fire characteristics and post-fire effects. *Int. J.Wildland Fire* **2006**, *15*, 319–345.

16. Csiszar, I.; Denis, L.; Giglio, L.; Justice, C.O.; Hewson, J. Global fire activity from two years of MODIS data. *Int. J. Wildland Fire* **2005**, *14*, 117–130.

17. Chuvieco, E.; Congalton, R.G. Mapping and inventory of forest fires from digital processing of TM data. *Geocarto Int.* **1988**, *3*, 41–53.

18. Duncan, B.W.; Shao, G.; Adrian, F.W. Delineating a managed fire regime and exploring its relationship to the natural fire regime in East Central Florida, USA: A remote sensing and gis approach. *Forest Ecol. Manag.* **2009**, *258*, 132–145.

19. Barbosa, P.M.; Grégoire, J.-M.; Pereira, J.M.C. An algorithm for extracting burned areas from time series of AVHRR GAC data applied at a continental scale. *Remote Sens. Environ.* **1999**, *69*, 253–263.

20. Roy, D.P.; Boschetti, L.; Justice, C.O.; Ju, J. The collection 5 modis burned area product—Global evaluation by comparison with the MODIS active fire product. *Remote Sens. Environ.* **2008**, *112*, 3690–3707.

21. Justice, C.O.; Giglio, L.; Korontzi, S.; Owens, J.; Morisette, J.T.; Roy, D.; Descloitres, J.; Alleaume, S.; Petitcolin, F.; Kaufman, Y. The MODIS fire products. *Remote Sens. Environ.* **2002**, *83*, 244–262.

22. Tansey, K.; Grégoire, J.-M.; Defourny, P.; Leigh, R.; Pekel, J.-F.; van Bogaert, E.; Bartholomé, E. A new, global, multi-annual (2000–2007) burnt area product at 1 km resolution. *Geophys. Res. Lett.* **2008**, doi:10.1029/2007GL031567.

23. Carmona-Moreno, C.; Belward, A.; Malingreau, J.-P.; Hartley, A.; Garcia-Alegre, M.; Antonovskiy, M.; Buchshtaber, V.; Pivovarov, V. Characterizing interannual variations in global fire calendar using data from earth observing satellites. *Glob. Chang. Biol.* **2005**, *11*, 1537–1555.

24. Xie, Y.; Sha, Z.; Yu, M. Remote sensing imagery in vegetation mapping: A review. *J. Plant Ecol.* **2008**, *1*, 9–23.

25. Salvador, R.; Valeriano, J.; Pons, X.; Diaz-Delgado, R. A semi-automatic methodology to detect fire scars in shrubs and evergreen forests with Landsat MSS time series. *Int. J. Remote Sens.* **2000**, *21*, 655–671.

26. Irons, J.R.; Dwyer, J.L.; Barsi, J.A. The next Landsat satellite: The Landsat data continuity mission. *Remote Sens. Environ.* **2012**, *122*, 11–21.

27. Chuvieco, E.; Martín, M.P.; Palacios, A. Assessment of different spectral indices in the red-near-infrared spectral domain for burned land discrimination. *Int. J. Remote Sens.* **2002**, *23*, 5103–5110.

28. Loboda, T.; O'Neal, K.J.; Csiszar, I. Regionally adaptable dNBR-based algorithm for burned area mapping from MODIS data. *Remote Sens. Environ.* **2007**, *109*, 429–442.

29. Maingi, J.K.; Henry, M.C. Factors influencing wildfire occurrence and distribution in eastern Kentucky, USA. *Int. J. Wildland Fire* **2007**, *16*, 23–33.

30. Quintano, C.; Fernández-Manso, A.; Fernández-Manso, O.; Shimabukuro, Y.E. Mapping burned areas in mediterranean countries using spectral mixture analysis from a uni-temporal perspective. *Int. J. Remote Sens.* **2006**, *27*, 645–662.

31. Koutsias, N.; Karteris, M. Burned area mapping using logistic regression modeling of a single post-fire Landsat-5 thematic mapper image. *Int. J. Remote Sens.* **2000**, *21*, 673–687.

32. Chuvieco, E.; Ventura, G.; Martín, M.P.; Gómez, I. Assessment of multitemporal compositing techniques of MODIS and AVHRR images for burned land mapping. *Remote Sens. Environ.* **2005**, *94*, 450–462.

33. Al-Rawi, K.R.; Casanova, J.L.; Calle, A. Burned area mapping system and fire detection system, based on neural networks and NOAA-AVHRR imagery. *Int. J. Remote Sens.* **2001**, *22*, 2015–2032.

34. Cao, X.; Chen, J.; Matsushita, B.; Imura, H.; Wang, L. An automatic method for burn scar mapping using support vector machines. *Int. J. Remote Sens.* **2009**, *30*, 577–594.

35. Katagis, T.; Gitas, I.Z.; Toukiloglou, P.; Veraverbeke, S.; Goossens, R. Trend analysis of medium- and coarse-resolution time series image data for burned area mapping in a mediterranean ecosystem. *Int. J. Wildland Fire* **2014**, doi:10.1071/WF12055.

36. Bastarrika, A.; Chuvieco, E.; Martin, M.P. Automatic burned land mapping from MODIS time series images: Assessment in mediterranean ecosystems. *IEEE Trans. Geosci. Remote Sens.* **2011**, *49*, 3401–3413.

37. Mitri, G.H.; Gitas, I.Z. A semi-automated object-oriented model for burned area mapping in the mediterranean region using Landsat-TM imagery. *Int. J. Wildland Fire* **2004**, *13*, 367–376.

38. Bastarrika, A.; Chuvieco, E.; Mart ń, M.P. Mapping burned areas from Landsat TM/ETM+ data with a two-phase algorithm: Balancing omission and commission errors. *Remote Sens. Environ.* **2011**, *115*, 1003–1012.

39. Oliveira, S.L.J.; Pereira, J.M.C.; Carreiras, J.M.B. Fire frequency analysis in Portugal (1975–2005), using Landsat-based burnt area maps. *Int. J. Wildland Fire* **2012**, *21*, 48–60.

40. Benz, U.C.; Hofmann, P.; Willhauck, G.; Lingenfelder, I.; Heynen, M. Multi-resolution, object-oriented fuzzy analysis of remote sensing data for GIS-ready information. *ISPRS J. Photogramm. Remote Sens.* **2004**, *58*, 239–258.

41. Blaschke, T. Object based image analysis for remote sensing. *ISPRS J. Photogramm. Remote Sens.* **2010**, *65*, 2–16.

42. Hay, G.J.; Castilla, G.; Wulder, M.A.; Ruiz, J.R. An automated object-based approach for the multiscale image segmentation of forest scenes. *Int. J. Appl. Earth Obs. Geoinf.* **2005**, *7*, 339–359.

43. Gitas, I.Z.; Mitri, G.H.; Ventura, G. Object-based image classification for burned area mapping of Creus Cape, Spain, using NOAA-AVHRR imagery. *Remote Sens. Environ.* **2004**, *92*, 409–413.

44. Mitri, G.H.;Gitas, I.Z. Fire type mapping using object-based classification of Ikonos imagery. *Int. J. Wildland Fire* **2006**, *15*, 457–462.

45. Polychronaki, A.; Gitas, I.Z. Burned area mapping in greece using SPOT-4 HRVIR images and object-based image analysis. *Remote Sens.* **2012**, *4*, 424–438.

46. Gitas, I. Geographical Information Systems and Remote Sensing in Mapping and Monitoring Fire-Altered Forest Landscapes. Ph.D. Dissertation, Department of Geography, University of Cambridge, Cambridge, UK, 1999.

47. Makedos, I. The Pinus Brutia Forest of Thasos. In *Pinus Halepensis and Pinus Brutia Forests (Ecology, Management and Development)*; Papanastasis, V., Ed.; Hellenic Association of Foresters: Chalkida, Greece, 1987.

48. Chander, G.; Markham, B.L.; Helder, D.L. Summary of current radiometric calibration coefficients for Landsat MSS, TM, ETM+, and EO-1 ALI sensors. *Remote Sens. Environ.* **2009**, *113*, 893–903.

49. Chavez, P.S.J. Radiometric calibration of Landsat thematic mapper multispectral images. *Photogramm. Eng. Remote Sens.* **1989**, *55*, 1285–1294.

50. Song, C.; Woodcock, C.E.; Seto, K.C.; Lenney, M.P.; Macomber, S.A. Classification and change detection using Landsat TM data: When and how to correct atmospheric effects? *Remote Sens. Environ.* **2001**, *75*, 230–244.

51. Baatz, M.; Benz, U.; Dehghani, S.; Heynen, M.; Holtje, A.; Hofmann, P.; Lingenfelder, I.; Mimler, M.; Sohlbach, M.; Weber, M. *eCognition Professional User Guide 4*; Definiens Imaging: Munich, Germany, 2004.

52. Congalton, R.G. A review of assessing the accuracy of classifications of remotely sensed data. *Remote Sens. Environ.* **1991**, *37*, 35–46.

53. Pontius, R., Jr.; Boersma, W.; Castella, J.-C.; Clarke, K.; Nijs, T.; Dietzel, C.; Duan, Z.; Fotsing, E.; Goldstein, N.; Kok, K.; *et al.* Comparing the input, output, and validation maps for several models of land change. *Ann. Reg. Sci.* **2008**, *42*, 11–37.

54. Pontius, R.G.; Millones, M. Death to kappa: Birth of quantity disagreement and allocation disagreement for accuracy assessment. *Int. J. Remote Sens.* **2011**, *32*, 4407–4429.

55. Czaplewski, R.L. Statistical Design and Methodological Considerations for the Accuracy Assessment of Maps of Forest Condition. In *Remote Sensing of Forest Environments: Concepts and Case Studies*; Wulder, M.A., Franklin, S.E., Eds.; Kluwer Academic: Boston, MA, USA, 2003; pp. 115–141.

56. Radoux, J.; Bogaert, P.; Fasbender, D.; Defourny, P. Thematic accuracy assessment of geographic object-based image classification. *Int. J. Geogr. Inf. Sci.* **2010**, *25*, 895–911.

57. Key, C.H. Ecological and sampling constraints on defining landscape fire severity. *Fire Ecol.* **2006**, *2*, 178–203.

58. Key C.; Benson, N. Landscape Assessment: Ground Measure of Severity; the Composite Burn Index, and Remote Sensing of Severity, the Normalized Burn Index. In *FIREMON: Fire Effects Monitoring and Inventory System*; Lutes, D., Keane, R., Caratti, J., Key, C., Benson, N., Sutherland, S., Grangi, L., Eds.; General Technical Report RMRS-GTR-164-CD LA; USDA Forest Service, Rocky Mountains Research Station: Ogden, UT, USA, 2006; pp. 1–51.

59. Chafer, C.J.N.M.M.E. The post-fire measurement of fire severity and intensity in the christmas 2001 Sidney wildfires. *Int. J. Wildland Fire* **2004**, *13*, 227–240.